Gray matter microglial activation in relapsing vs progressive MS

A [F-18]PBR06-PET study

Tarun Singhal, MD, Kelsey O'Connor, BS, Shipra Dubey, PhD, Hong Pan, PhD, Renxin Chu, PhD, Shelley Hurwitz, PhD, Steven Cicero, BS, Shahamat Tauhid, MD, David Silbersweig, MD, Emily Stern, MD, Marie Kijewski, DSc, Marcelo DiCarli, MD, Howard L. Weiner, MD, and Rohit Bakshi, MD, MA

Correspondence
Dr. Singhal
tsinghal@bwh.harvard.edu

Abstract

Objective

To determine the value of [F-18]PBR06-PET for assessment of microglial activation in the cerebral gray matter in patients with MS.

Methods

Twelve patients with MS (7 relapsing-remitting and 5 secondary progressive [SP]) and 5 healthy controls (HCs) had standardized uptake value (SUV) PET maps coregistered to 3T MRI and segmented into cortical and subcortical gray matter regions. SUV ratios (SUVRs) were global brain normalized. Voxel-by-voxel analysis was performed using statistical parametric mapping (SPM). Normalized brain parenchymal volumes (BPVs) were determined from MRI using SIENAX.

Results

Cortical SUVRs were higher in the hippocampus, amygdala, midcingulate, posterior cingulate, and rolandic operculum and lower in the medial-superior frontal gyrus and cuneus in the MS vs HC group (all $p < 0.05$). Subcortical gray matter SUVR was higher in SPMS vs RRMS (+10.8%, $p = 0.002$) and HC (+11.3%, $p = 0.055$) groups. In the MS group, subcortical gray matter SUVR correlated with the Expanded Disability Status Scale (EDSS) score (r = 0.75, $p = 0.005$) and timed 25-foot walk (T25FW) (r = 0.70, $p = 0.01$). Thalamic SUVRs increased with increasing EDSS scores (r = 0.83, $p = 0.0008$) and T25FW (r = 0.65, $p = 0.02$) and with decreasing BPV (r = −0.63, $p = 0.03$). Putaminal SUVRs increased with increasing EDSS scores (0.71, $p = 0.009$) and with decreasing BPV (r = −0.67, $p = 0.01$). On SPM analysis, peak correlations of thalamic voxels with BPV were seen in the pulvinar and with the EDSS score and T25FW in the dorsomedial thalamic nuclei.

Conclusions

This study suggests that [F-18]PBR06-PET detects widespread abnormal microglial activation in the cerebral gray matter in MS. Increased translocator protein binding in subcortical gray matter regions is associated with brain atrophy and may link to progressive MS.

Glossary

AAL = automated anatomic labeling; **BPV** = brain parenchymal volume; **C-SUVR** = total cortical gray standardized uptake value ratio; **EDSS** = Expanded Disability Status Scale; **HC** = healthy control; **RCP** = radiochemical purity; **ROI** = region of interest; **RR** = relapsing-remitting; **SC-SUVR** = total subcortical gray matter standardized uptake value ratio; **SP** = secondary progressive; **SUVR** = standardized uptake value ratio; **T25FW** = timed 25-foot walk; **TSPO** = translocator protein.

There has been increasing recognition of gray matter pathology in MS since the seminal histopathologic description of gray matter plaques by Brownell et al. in 1962.[1,2] Microglial activation and neuronal loss have been demonstrated in gray matter MS lesions and normal-appearing gray matter.[1] Brain atrophy has been associated with disease progression,[3] and regional gray matter loss has been associated with specific clinical impairment.[4] However, the mechanism of brain atrophy in MS is not clear. There is a need to better understand the role of gray matter microglial activation in disease pathogenesis.

[F-18]PBR06 [N-(2,5-dimethoxybenzyl)-2-(18)F-fluoro-N-(2-phenoxyphenyl)acetamide] is a second-generation PET radioligand, targeting the 18-kDa-translocator protein (TSPO), which is overexpressed on activated microglia/macrophages.[5] The longer physical half-life of F-18 (110 minutes) as compared to C-11 (20 minutes, used to label conventional TSPO ligands such as [C-11]PK11195) enables improved image quality, increased signal-to-noise ratio, and higher clinical feasibility.[6] Strong correlations of [F-18]PBR06-binding with both CD68 expression and TSPO-antibody reactivity have been demonstrated in multiple disease models.[7,8] [F-18]PBR06 has been studied in healthy human volunteers but not in MS, except for our recent study on white matter microglial activation in MS.[9] The aims of this pilot study were to assess differences in microglial activity in the cortical and subcortical gray matter regions between patients with MS and healthy controls (HCs), and between patients with relapsing-remitting (RR) and secondary progressive (SP) MS, and to identify any association of microglial activation with brain atrophy and physical disability using [F-18]PBR06 PET.

Methods

Participants

Eighteen MS and 7 HC participants were initially enrolled. Two MS and 2 HC participants were low-affinity binders and were excluded from the study (see the Genotyping section below). Four additional MS participants subsequently lost interest or were lost to follow-up after initial screening. Ultimately, 12 patients with MS (7 RR and 5 SP; 8 women [67%]) and 5 HC participants (3 women, 60%) completed the study. Participant characteristics are summarized in table 1 and detailed for each participant in table 2.

Clinical course (RR or SP) was initially determined by the treating neurologists and documented in the patient's chart.

The clinical course was subsequently verified by TS by chart review, and determination of SPMS was based on the 2013 International Advisory Committee on Clinical Trials of MS criteria.[10] The inclusion criteria required patients with SP to have demonstrated an increase in the Expanded Disability Status Scale (EDSS) score by 1.0 or 0.5, if the baseline EDSS score was <5 or ≥5.5, respectively, in the last 1 year. Patients with RR were included if there was a history of a clinical relapse in the last 1 year or if there was evidence of a new or enlarging T2 bright lesion on MRI or a gadolinium-enhancing lesion on T1-weighted MRI. Patients were excluded if they received corticosteroids in the last 1 month before PET scanning. The median time interval between formal clinical assessment and PET scanning was 5.1 (range 1.1–25.6) weeks. There was no history of relapses or clinical deterioration between the clinical visits immediately before and after the PET scanning.

Standard protocol approvals, registrations, and patient consents

The study is registered on clinicaltrials.gov with the clinical trial identifier number, NCT02649985. The study was approved by the Institutional Review Board and Radioactive Drug Research Committee at Brigham and Women's Hospital; written informed consent was obtained from all participants.

Genotyping

Blood samples drawn on the initial screening visit were genotyped for DNA polymorphism of the *TSPO* gene on chromosome 22q13.2, using a TaqMan assay. High-affinity and medium-affinity binders were included in the study, whereas low-affinity binders (4 participants, including 2 MS and 2 HC) were excluded. Among the 12 included patients with MS, 7 (58%) were high-affinity and 5 were medium-affinity binders, and among the HCs, 2 (40%) were high-affinity and 3 were medium-affinity binders (table 2). There were no statistically significant differences in the TSPO-binding affinity distribution between the 2 groups (table 1).

Production of radiopharmaceuticals

[F-18]PBR06 was produced in the Nuclear Medicine/Biomedical Imaging Research Core facility at our hospital according to standardized procedures. The product was purified by high-pressure liquid chromatography and sterilized by a 0.22-μm membrane filter. The final product was dispensed in an isotonic solution that was sterile and pyrogen-free for IV administration. The radiochemical purity (RCP) of radiopharmaceuticals was determined using high-pressure

Table 1 Participant characteristics: summary

	MS (N = 12)	HC (N = 5)	*p* Value
Age (y)	42 ± 11.7	37.8 ± 13.3	0.60
Sex distribution	7 F, 5 M	3 F, 2 M	0.95
TSPO-binding affinity	7 high, 5 medium	2 high, 3 medium	0.49
Median EDSS score	3.5		
T25FW (s)	7.2 ± 3.7		

Abbreviations: EDSS = Expanded Disability Status Scale; HC = healthy control; T25FW = timed 25-foot walk; TSPO = translocator protein.
Data are mean ± SD, unless otherwise indicated.

liquid chromatography. The organic solvents were determined using gas chromatography. The RCP of the radiopharmaceuticals was >95%.

MRI acquisition and analysis

All participants underwent MRI on the same scanner (Siemens 3T Skyra, Erlangen, Germany) using the same high-resolution acquisition protocol as previously described.[11–13] This included a 2D T1-weighted spin-echo axial series (the repetition time = 611–943 ms, and echo time = 7.9 ms, voxel size = 0.43 × 0.43 × 3 mm) and a 3D magnetization-prepared rapid gradient-echo series (voxel size 1 mm^3). The latter images were applied to a fully automated algorithm to derive normalized whole brain parenchymal volume (BPV) (SIENAX, v. 5.0; Analysis Group, fsl.fmrib.ox.ac.uk), using our previously described method.[14]

PET acquisition and analysis

[F-18]PBR06 was injected as a bolus injection for PET scanning using an IV catheter into the radial antecubital or other arm or hand vein; images were acquired in a list mode acquisition mode using a high-resolution PET/CT scanner (GE Discovery ECAT, Waukesha, WI).

For each participant, using the PNEURO 3.8 platform (PMOD Technologies, Zurich, Switzerland; pmod.com), summed [F-18]PBR06 PET images obtained between 60 and 90 minutes after tracer injection were coregistered to MRI, and segmentation of images into brain regions was based on the automated anatomical labeling (AAL) template within the PNEURO utilities suite.[15] Two regions of interest (ROIs) were derived after collapsing the supratentorial AAL template output: (1) a supratentorial cortical region of interest representing the union of 41 regions in each hemisphere, including the amygdala; (2) a subcortical gray matter ROI representing the union of the thalamus, caudate, putamen, and globus

Table 2 Participant characteristics: detailed

Participant number	Sex	Age (y)	TSPO-binding affinity	Group	Disease duration (y)	Current DMT	EDSS score	T25FW (s)
1	F	37	High	RR	5.2	Fingolimod	4	6.1
2	M	37	High	RR	19.6	Rituximab	3	5.8
3	F	34	Medium	RR	4.8	Fingolimod	1	3.4
4	M	32	Medium	RR	11.9	Fingolimod	1	4
5	F	23	High	RR	8.2	Natalizumab	1.5	4.8
6	F	41	High	RR	9.6	Fingolimod	1.5	5.0
7	F	27	Medium	RR	3.5	Fingolimod	2	4.8
8	M	52	Medium	SP	14.9	Rituximab	6.5	8.5
9	M	53	High	SP	19	Rituximab	6	8.5
10	F	59	Medium	SP	19	Glatiramer acetate	6	12.1
11	F	59	High	SP	19	None	6.5	17.1
12	F	50	High	SP	17	Rituximab	4.5	6.8
13	M	25	Medium	HC				
14	F	45	High	HC				
15	M	60	Medium	HC				
16	F	25	High	HC				
17	F	34	Medium	HC				

Abbreviations: Disease duration is time from the onset of first symptoms; DMT = disease-modifying treatment; EDSS = Expanded Disability Status Scale; RR = relapsing-remitting; SP = secondary progressive; TSPO = translocator protein; T25FW = timed 25-foot walk.

pallidus. To account for interparticipant differences, a total cortical gray matter and a total subcortical gray matter standardized uptake value ratio (SUVR) (C-SUVR and SC-SUVR, respectively) were calculated for each participant based on normalization of the individual region's SUV_{60-90} to the global brain SUV_{60-90}. To assess the appropriateness of using global SUV_{60-90} as a reference for normalization, global SUV_{60-90} was compared between the MS and HC groups and showed no significant difference (0.87 ± 0.20 vs 0.73 ± 0.13, p = 0.22). SUVRs for individual supratentorial AAL template ROIs (averages of right and left) were also obtained and assessed for group comparisons (a complete list of ROIs obtained is shown in table 1, links.lww.com/NXI/A123). Because the subcortical gray matter showed significant correlations with disability, the correlations of PET uptake in subregions within this ROI (thalamus, caudate, putamen, and globus pallidus) were further investigated. To gain additional insight into the topographic relevance of subcortical gray matter changes, a second set of post hoc analyses was performed. [F-18]PBR06 PET SUV images were processed using SPM12 software (the Wellcome Institute of Cognitive Neurology, London, UK; fil.ion.ucl.ac.uk/spm/software/).[16] Stereotactic normalization of PET images to the Montreal Neurologic Institute version of Talairach space was performed. Voxel-by-voxel whole-brain multiple linear regression modeling was applied to individual scans.[6] Contrast-effect images were then progressed into group-level models. Parametric images were generated to demonstrate the age- and sex-adjusted correlations of thalamic PET uptake with the EDSS score, timed 25-foot walk (T25FW), and BPV in the MS group. All image analyses were performed blinded to study group and clinical scores.

Statistical analysis

For the primary analysis, the exact Wilcoxon-Mann-Whitney test was used to assess the statistical significance of mean differences in SUVRs. For age-adjusted comparisons between SPMS vs RRMS and HC groups, analysis of covariance was used to compare groups while including age in the model. To assess associations, Spearman correlation coefficient r's were calculated. This pilot study was exploratory in nature with a small sample size that is not based on formal sample size calculations, and results should be considered hypothesis generating. Therefore, no correction was made for multiple statistical tests.

Data availability

Any unpublished study data will be available for sharing with any qualified investigators after due anonymization.

Results

Group comparisons in the cortical and subcortical gray matter: MS vs HC

There was no significant difference between MS and HC groups in the total cortical (1.09 ± 0.04 vs 1.11 ± 0.07,

p = 0.72) and subcortical gray matter regions (0.93 ± 0.06 vs 0.88 ± 0.06, p = 0.23) (figure 1, A and B). However, the following cortical subregions showed increased SUVRs in MS vs HC groups (figure 1C): the rolandic operculum (1.031 ± 0.119 vs 0.856 ± 0.053, mean + 20.4%, p = 0.006), midcingulate (1.131 ± 0.097 vs 1.013 ± 0.049, +11.6%, p = 0.01), posterior cingulate (1.106 ± 0.158 vs 0.961 ± 0.074, +15.1%, p = 0.03), hippocampus (1.020 ± 0.106 vs 0.880 ± 0.096, +15.9%, p = 0.03), and amygdala (1.037 ± 0.075 vs 0.898 ± 0.125, +15.5%, p = 0.01). On the other hand, decreased SUVRs were seen in the MS vs HC (figure 1D) in the cuneus (1.128 ± 0.108 vs 1.370 ± 0.105, −17.7%, p = 0.001) and medial-superior frontal gyrus (1.086 ± 0.103 vs 1.291 ± 0.178, −15.9%, p = 0.048). No other supratentorial regions from the AAL template showed a significant difference between MS and HC groups.

Group comparisons in the cortical and subcortical gray matter between SPMS, RRMS, and HC groups

On univariate analysis, total subcortical gray matter SUVR (SC-SUVR) was higher in the SPMS vs RRMS (0.988 ± 0.029 vs 0.891 ± 0.053, +10.8%, p = 0.002). The effect sizes and age-adjusted p values for SPMS vs RRMS were 2.07 and 0.03 and those for SPMS vs HC were 1.87 and 0.10, respectively (figure 1E). On the other hand, total cortical SUVR was not significantly different among the SPMS, RRMS, and HC groups (figure 1F).

Age-adjusted group comparisons in subregions of the subcortical gray matter between SPMS, RRMS, and HC groups

In terms of subregions of the subcortical gray matter, thalamic SUVRs were higher in SPMS vs RRMS (1.250 ± 0.018 vs 1.099 ± 0.084, +13.7%, p = 0.03) and SPMS vs HC (1.250 ± 0.018 vs 1.087 ± 0.060, +15.0%, p = 0.003) (figure 1G). Putaminal SUVR was 0.974 ± 0.015 vs 0.892 ± 0.052 in SP vs HC groups (+9.2%) but did not attain statistical significance (p = 0.06).

Age-adjusted group comparisons in subregions of the cortical gray matter between SPMS, RRMS, and HC groups

In terms of subregions of the cortical gray matter, increased SUVRs in the SPMS vs HC group were seen in the rolandic operculum (1.053 ± 0.087 vs 0.856 ± 0.053, +23.0%, p = 0.008), hippocampus (1.068 ± 0.093 vs 0.88 ± 0.096, +21.3%, p = 0.04), midcingulate (1.132 ± 0.048 vs 1.013 ± 0.049, +11.7%, p = 0.002), parahippocampus (0.976 ± 0.048 vs 0.854 ± 0.049, +14.3%, p = 0.02), olfactory cortex (1.035 ± 0.197 vs 0.795 ± 0.404, +30.2%, p = 0.01), insula (1.068 ± 0.096 vs 0.95 ± 0.063, +12.4%, p = 0.04), and middle temporal gyrus (1.15 ± 0.035 vs 1.131 ± 0.07, +1.7%, p = 0.04) On the other hand, decreased SUVRs in SPMS vs HC groups were seen in the dorsolateral superior frontal gyrus (1.057 ± 0.116 vs 1.303 ± 0.23, −18.8%, p = 0.01), middle frontal gyrus (1.133 ± 0.062 vs 1.25 ± 0.077, −9.4%, p = 0.047), and supplementary motor area (1.057 ± 0.161 vs 1.474 ± 0.49, −28.2%, p = 0.02) Comparison of the RRMS and HC groups revealed increased

Figure 1 Group differences of SUVRs in cortical and subcortical gray matter regions
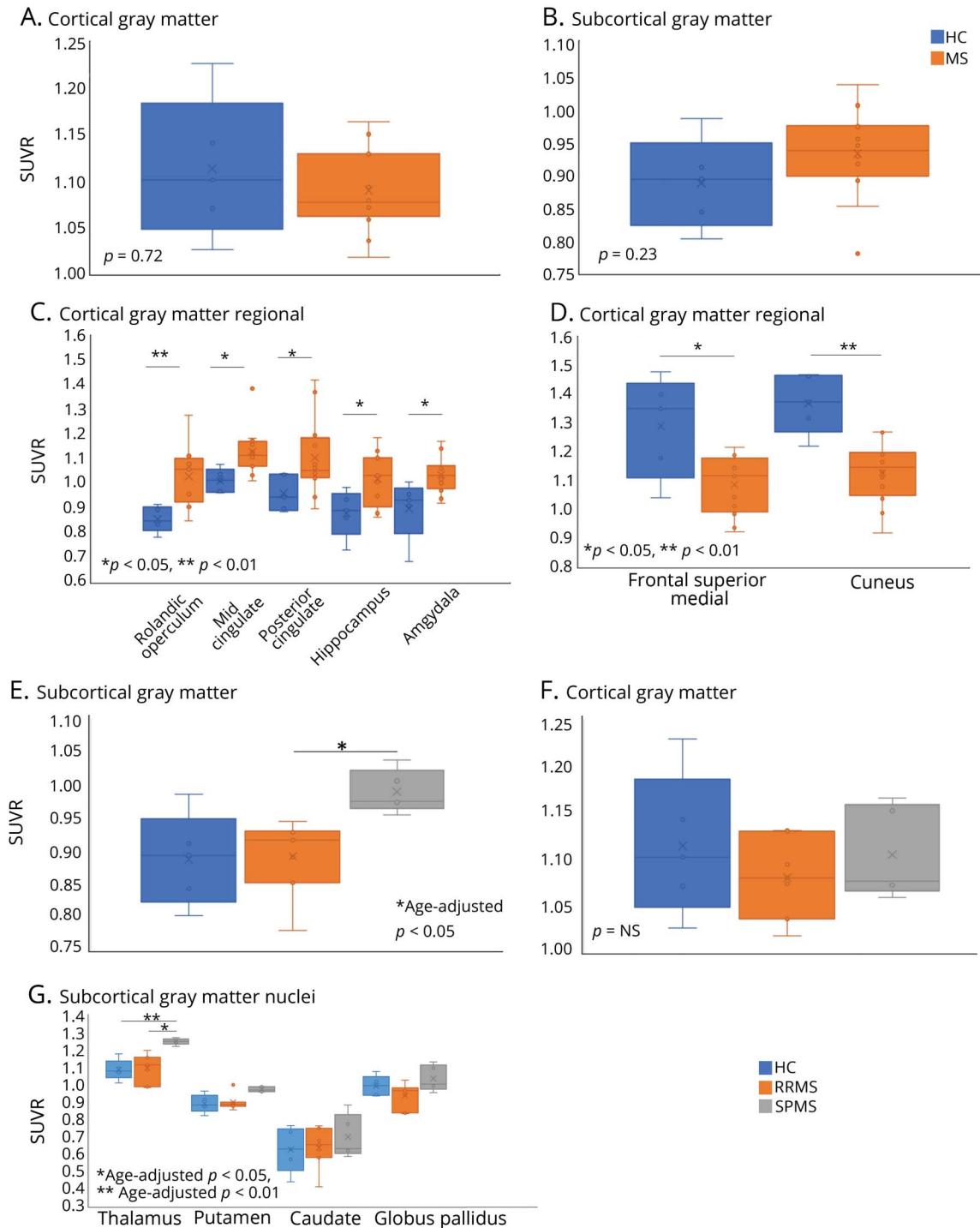
Differences in (A and B) overall cortical and subcortical gray matter ROIs between MS vs HC, (C and D) cortical subregions between MS vs HC, (E and F) overall subcortical and cortical gray matter ROIs among SPMS, RRMS, and HC groups, (G) subcortical subregions (thalamus, putamen, caudate, and globus pallidus) among SPMS, RRMS, and HC groups. Open circles in the box plots indicate individual participants, "x" represents mean, horizontal line within box represents median, ends of whiskers represent minimum and maximum values, and closed circle represents outliers. HC = healthy control; ROI = region of interest; RR = relapsing-remitting; SP = secondary progressive; SUVR = standardized uptake value ratio.

SUVRs in the rolandic operculum (1.014 ± 0.142 vs 0.856 ± 0.053, +18.458%, $p = 0.03$) and decreased SUVRs in the cuneus (1.143 ± 0.078 vs 1.37 ± 0.105, −16.569%, $p = 0.005$). The supramarginal gyrus showed increased SUVRs (1.247 ± 0.043 vs 1.177 ± 0.085, +6%, $p = 0.007$) in the SPMS vs RRMS group. The effect sizes for the complete list of subgroup comparisons for the cortical and subcortical subregions are provided in table 2, links.lww.com/NXI/A123.

Relationship between PET and physical disability

In the MS group, there were significant correlations between the EDSS score and subcortical gray matter SUVR (r = 0.74, p = 0.005) (figure 2A) but not cortical SUVR (r = 0.05, p = 0.87). There were significant correlations between the EDSS score and SUVR in the thalamus (r = 0.83, p = 0.0008) and putamen (r = 0.71, p = 0.0089) (figures 2B and 3A). No significant correlations were seen between the EDSS score and SUVR in the caudate (r = 0.28, p = 0.37) or globus pallidus (r = 0.42, p = 0.17). On SPM analysis, age- and sex-adjusted correlations were seen in the thalamus between the EDSS score and PET uptake (p = 0.02). The peak thalamic voxels showing significant correlation with the EDSS score in the thalamus were localized to the dorsomedial nucleus (figure 3B).

Relationship between PET and T25FW

In the MS group, there were significant correlations between T25FW and subcortical gray matter SUVRs (r = 0.70, p = 0.01) (figure 2C) but not cortical SUVR. There was a significant correlation between T25FW and SUVR in the thalamus (r = 0.65, p = 0.02) (figures 2D and 3A). The correlation coefficient between T25FW and putaminal SUVR was 0.57 but did not attain statistical significance (p = 0.053) (figure 2D). No significant correlations were seen between T25FW and SUVR in the caudate (r = 0.44, p = 0.15) and globus pallidus (r = 0.40, p = 0.19). On SPM analysis, age- and sex-adjusted correlations were seen in the thalamus between T25FW and PET uptake (p = 0.02). The peak thalamic voxels showing significant correlation with T25FW in the thalamus were localized to the dorsomedial nucleus (figure 3C).

Figure 2 Correlations of subcortical gray matter SUVRs with the EDSS score, T25FW, and BPV in MS
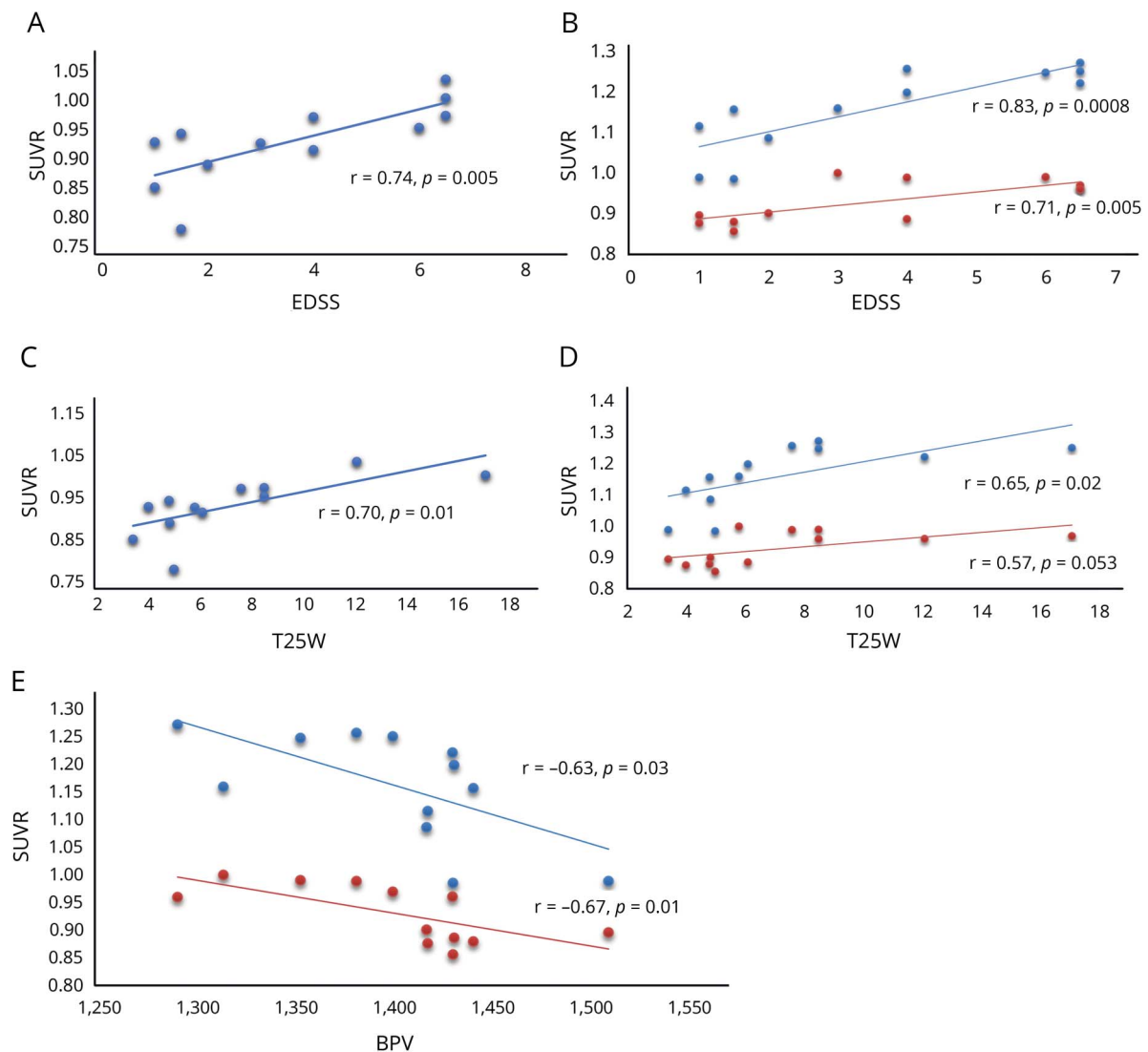
Correlations in the MS group of (A) subcortical gray matter SUVR vs EDSS score, (B) thalamic and putaminal SUVR vs EDSS score, (C) subcortical gray matter SUVR vs T25FW, (D) thalamic and putaminal SUVR vs T25FW, and (E) thalamic and putaminal SUVR vs BPV. In panels (A) and (C), blue dots represent subcortical gray matter values. In panels (B), (D), and (E), blue dots represent thalamic values and red dots represent putaminal values. BPV = normalized brain parenchymal volume; EDSS = Expanded Disability Status Scale; SUVR = standardized uptake value ratio; T25FW = timed 25-foot walk.

Figure 3 [F-18]PBR06 PET SUV images and statistical parametric maps in subjects with MS
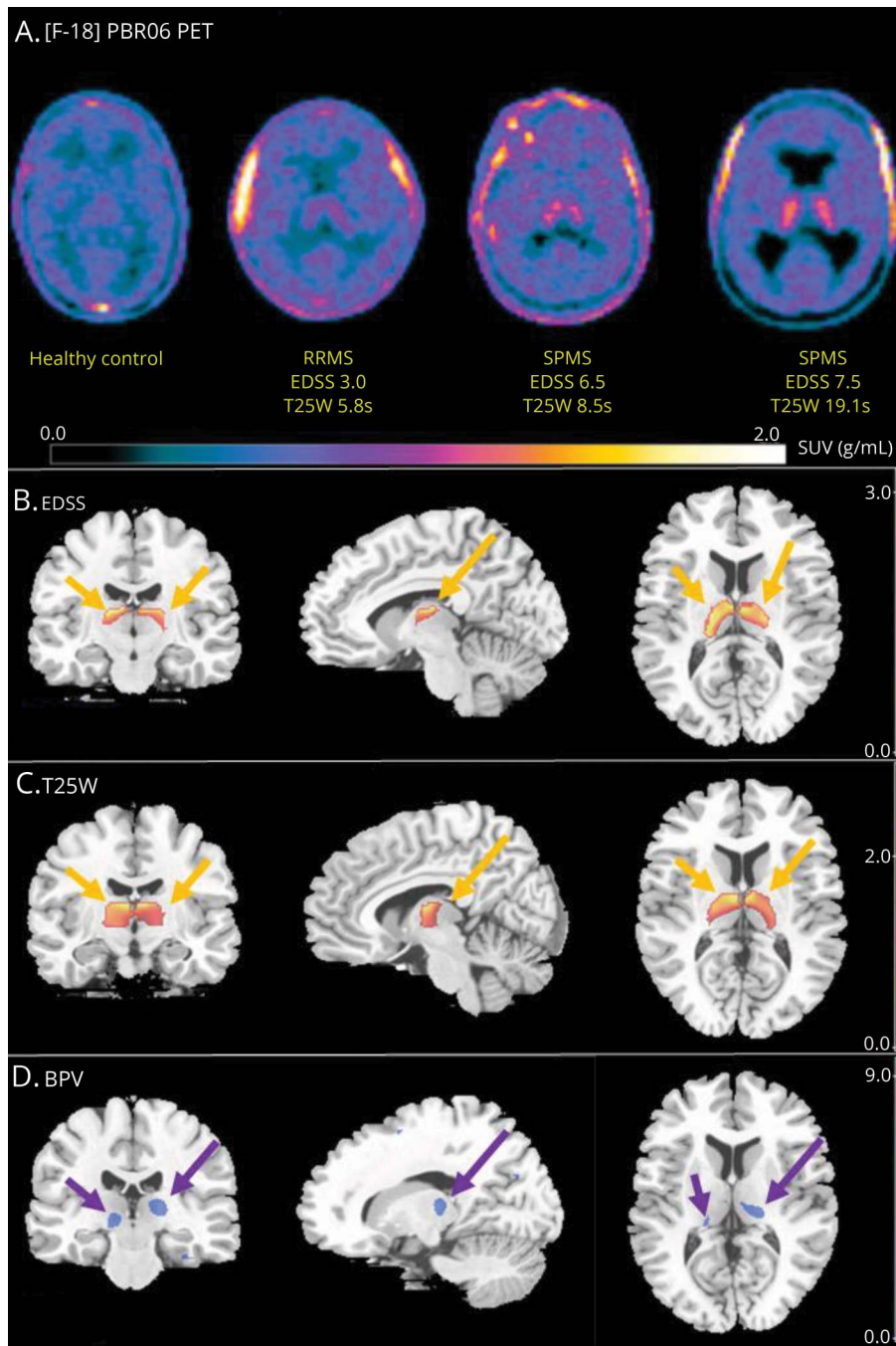
(A) [F-18]PBR06 PET sample images of an individual healthy control and patients with RRMS or SPMS. (A) SUV images were summed from 60 to 90 minutes after radiotracer injection. Images showing higher thalamic uptake with higher disability (SUVRs 1.08, 1.16, 1.24, and 1.4, respectively). All participants are age-matched, high-affinity binders. (B–D) Age- and sex-adjusted SPM analysis showing correlations in the MS group of PET uptake with the EDSS score, T25FW, and BPV in the thalamus. The color bars represent T-scores, and the colored highlights show the localization of peak clusters of voxels, demonstrating increases with the EDSS score and T25FW in the dorsomedial nucleus of the thalamus (orange arrows) and a decrease with BPV in the pulvinar (purple arrows). BPV = normalized brain parenchymal volume; EDSS = Expanded Disability Status Scale; HC = healthy control; RR = relapsing-remitting; SP = secondary progressive; SUVR = standardized uptake value ratios; T25FW = timed 25-foot walk.

Relationship between PET and whole-brain volume

There was no significant correlation between overall cortical and subcortical gray matter SUVRs and BPV (r = 0.31, p = 0.32 and r = 0.38, p = 0.22, respectively). However, correlation analysis revealed a relationship between decreasing BPV and increasing SUVRs in the thalamus (r = −0.63, p = 0.03) and putamen (r = −0.67, p = 0.01) (figure 2E). No significant correlations were seen between BPV and SUVR in the caudate (r = 0.21, p = 0.51) and globus pallidus (r = −0.29, p = 0.36).

On SPM analysis, peak thalamic voxels showing significant age- and sex-adjusted decreases in BPV with increasing PET uptake were localized to the pulvinar (p = 0.02) (figure 3D).

Discussion

The key findings of our pilot study are as follows: (1) Subcortical gray matter demonstrated higher microglial activation in patients with SPMS compared with patients with RRMS

and HCs, and this activation correlated with physical disability measures (EDSS score and T25FW) in patients with MS; (2) Thalamic and putaminal microglial activation primarily drove these findings in the subcortical gray matter, and thalamic microglial activation correlated with brain atrophy; (3) Regional cortical microglial activation in several limbic and paralimbic cortical regions (but not total cortical gray matter microglial activation) was increased in the MS group.

These PET findings underscore the role of microglial activation in progression of disease in MS with accumulation of microglial activation burden in SPMS, particularly in the subcortical gray matter. Gray matter microglial activation in MS has not been studied before using [F-18]PBR06, a longer-half-life PET tracer. There is an urgent need to identify an imaging biomarker linked to progressive MS, and our results suggest that [F-18]PBR06 PET is a promising technique in this regard. Increased microglial activation in SPMS has been previously reported using [C-11]PK11195 in the cortical gray matter[17] and using [C-11]PBR28 in cortical and subcortical gray matter regions,[18] but both [C-11]PK11195 and [C-11]PBR28 are short half-life PET tracers, which are not easily adapted for routine clinical use.

Our study demonstrates the correlation of thalamic microglial activation with brain atrophy, EDSS score, and T25FW suggesting a central role of thalamic neuroinflammation in the pathogenesis and disease progression in MS. Extensive pathologic changes have been demonstrated in the thalamus[19] that may also be related to the high thalamic iron content.[20] Thalamic elevation of myoinositol concentration, reflecting increased glial activity, has been reported in MS using magnetic resonance spectroscopy.[21] Thalamic atrophy is known to occur throughout the course of MS at an accelerated rate, compared with HCs,[22] and microglial activation may play a causative role in its development. This aspect is a key to understanding of the mechanism of brain atrophy in MS and requires further investigation. A previous PET study has demonstrated an association of cortical thinning with thalamic TSPO binding, using a C-11 labeled tracer.[18] Progressive reductions in thalamic and putaminal T2-hypointensity, suggesting increasing iron deposition, have been associated with clinical progression in a 4-year longitudinal study of patients with MS.[23] Increased thalamic TSPO binding in patients with SPMS[24] and in a separate cohort of 8 patients with RRMS, 3 with PPMS, and 1 with SPMS[25] compared with HCs has been described using [C-11]PK11195.[24,25] Similarly, several subcortical gray matter regions, including the thalamus and putamen, demonstrated demyelination, microglial activation, and neurodegeneration on pathologic examination of brain sections from patients with MS compared with controls.[19] We found correlation of microglial activation in the dorsomedial thalamic nucleus with increasing disability and correlation of brain atrophy with microglial activation in the pulvinar. These findings are similar to a recent report of decreased magnetic susceptibility in the pulvinar in SPMS and in the rest of thalamus including the dorsomedial nucleus in patients with RRMS.[26]

Chronic microglial activation may lead to cellular injury and iron depletion from oligodendrocytes, accounting for PET findings and decreased magnetic susceptibility in these regions.[26]

Cortical gray matter findings of our study are consistent with pathologic and neuroimaging data available in the literature. Extensive hippocampal demyelination accompanied by microglial activation has been demonstrated on autopsy examination of MS brains.[27] Several of these specimens demonstrated involvement of both the hippocampus and parahippocampal cortices.[27,28] Hippocampal elevation of myoinositol concentration, reflecting increased glial activity, has been reported in MS using magnetic resonance spectroscopy.[21] Of interest, in an autopsy study of patients with SPMS, ectopic B-cell follicles were most frequently found in forebrain regions, including the temporal and cingulate cortex, and correlated with increased demyelination and parenchymal CD68$^+$ cells in proximity to these regions.[29] Regional brain atrophy patterns have been identified, and atrophy in temporal and cingulate cortical regions has been associated with cognitive changes in MS.[30] Other PET studies using C-11–labeled radioligands have shown similar results on cross-sectional comparison. Using [C-11]PK11195, spatially heterogeneous increases in TSPO binding were demonstrated in multiple cortical brain regions, including the parahippocampal and fusiform gyri.[17] Another PET study demonstrated increased hippocampal TSPO binding in MS vs HCs that correlated with depression scores and hippocampal functional connectivity measures.[31]

Of interest, the cuneus and medial-superior frontal gyrus showed reduced PET uptake in patients with MS in our study. This finding may represent a partial volume effect from severe atrophy in these regions or locally "burnt out" disease with chronic scar formation and requires further confirmation and evaluation in future studies.

The underlying mechanisms connecting cortical and subcortical microglial activation in MS are not clear. The relationship between cortical and thalamic pathology may be mediated via thalamocortical projection pathways. It is known that the "core" or C-type thalamic cells project to layer 4 of the cerebral cortex and "matrix" or M-type thalamic neurons project to the apical dendritic tufts in outermost cortical layer 1, which, in turn, is affected by the subpial gray matter lesions that are a specific aspect of MS pathology.[32] In addition, diffusion tensor fractional anisotropy values have been reported to be reduced in the cingulum, fornix, and uncinate fasciculus, along with thalamic and hippocampal atrophy, suggesting disruption of hippocampal-thalamic-prefrontal connections in patients with RRMS.[33]

Microglial activation may be a cause or effect of neurodegeneration,[34] and the cross-sectional nature of our study cannot definitively answer that question. Mechanistically, activated microglia can cause ongoing injury in non–antigen-

dependent manner, mediated via the production of cytokines, glutamate, oxygen radicals, nitric oxide, matrix proteases, and putative proapoptotic signals.[35,36] It has been shown that microglial activation correlates with neurofilament positive swellings at terminal ends of transected axons and dendrites in demyelinating lesions. In addition, the pattern of microglial targeting of neurons suggests neuronal damage via a process of synaptic stripping.[35,37] Neuronal apoptosis and atrophy may result from axonal transection and other neuronal or axonal damage. In cortical gray matter lesions, there microglia are not abundant, but they are highly activated.[38] Recently, CCR2+ monocytes were found to be necessary for the development of both type 2 intracortical and type 3 subpial gray matter lesions.[39]

The limitations of our pilot study include its small sample size and cross-sectional design. We did not correct for multiple comparisons while assessing statistical significance, and hence, our findings represent trends that require further confirmation. Increased microglial activation has been reported in the caudate on histopathologic examination but was not detected on PET in our study, which may be due to sample size or partial volume effects diluting the PET signal in an atrophied caudate nucleus. However, this is the first study of [F-18]PBR06 PET, assessing gray matter changes in MS, demonstrating potential value of this technique. The practical advantages of this longer half-life tracer have implications for its potential clinical use in the long term, and hence, larger studies with longitudinal design are needed to confirm and extend the findings of our pilot study.

This study suggests that [F-18]PBR06 PET detects widespread abnormal brain microglial activation in the cerebral gray matter in MS, and increased activation in subcortical gray matter regions is associated with brain atrophy and physical disability. Further studies of [F-18]PBR06 PET in MS are warranted.

Appendix Authors

Name	Location	Role	Contribution
Tarun Singhal, MD	Brigham and Women's Hospital, Harvard Medical School, Boston, MA, USA	Author	Designed and conceptualized the study; major role in the acquisition of data; analyzed and interpreted the data; drafted and revised the manuscript for intellectual content; and provided funding
Kelsey O'Connor, BS	Brigham and Women's Hospital, Harvard Medical School, Boston, MA, USA	Author	Major role in the acquisition of data and analyzed and interpreted the data
Shipra Dubey, PhD	Brigham and Women's Hospital, Harvard Medical School, Boston, MA, USA	Author	Designed and conceptualized the study and major role in the acquisition of data
Hong Pan, PhD	Brigham and Women's Hospital, Harvard Medical School, Boston, MA, USA	Author	Analyzed and interpreted the data and revised the manuscript for intellectual content
Renxin Chu, PhD	Brigham and Women's Hospital, Harvard Medical School, Boston, MA, USA	Author	Analyzed and interpreted the data
Shelley Hurwitz, PhD	Brigham and Women's Hospital, Harvard Medical School, Boston, MA, USA	Author	Analyzed and interpreted the data and revised the manuscript for intellectual content
Steven Cicero, BS	Brigham and Women's Hospital, Harvard Medical School, Boston, MA, USA	Author	Major role in the acquisition of data and analyzed and interpreted the data
Shahamat Tauhid, MD	Brigham and Women's Hospital, Harvard Medical School, Boston, MA, USA	Author	Analyzed and interpreted the data

Continued

Appendix *(continued)*

Name	Location	Role	Contribution
David Silbersweig, MD	Brigham and Women's Hospital, Harvard Medical School, Boston, MA, USA	Author	Analyzed and interpreted the data and revised the manuscript for intellectual content
Emily Stern, MD	Brigham and Women's Hospital, Harvard Medical School, Boston, MA, USA	Author	Designed and conceptualized the study; analyzed and interpreted the data; and revised the manuscript for intellectual content
Marie Kijewski, DSc	Brigham and Women's Hospital, Harvard Medical School, Boston, MA, USA	Author	Designed and conceptualized the study; analyzed and interpreted the data; and revised the manuscript for intellectual content
Marcelo DiCarli, MD	Brigham and Women's Hospital, Harvard Medical School, Boston, MA, USA	Author	Designed and conceptualized the study and revised the manuscript for intellectual content
Howard L. Weiner, MD	Brigham and Women's Hospital, Harvard Medical School, Boston, MA, USA	Author	Designed and conceptualized the study; revised the manuscript for intellectual content; and provided funding
Rohit Bakshi, MD, MA	Brigham and Women's Hospital, Harvard Medical School, Boston, MA, USA	Author	Designed and conceptualized the study; revised the manuscript for intellectual content; and provided funding

References

1. Calabrese M, Magliozzi R, Ciccarelli O, Geurts JJ, Reynolds R, Martin R. Exploring the origins of grey matter damage in multiple sclerosis. Nat Rev Neurosci 2015;16:147–158.
2. Brownell B, Hughes JT. The distribution of plaques in the cerebrum in multiple sclerosis. J Neurol Neurosurg Psychiatry 1962;25:315–320.
3. Fisher E, Lee JC, Nakamura K, Rudick RA. Gray matter atrophy in multiple sclerosis: a longitudinal study. Ann Neurol 2008;64:255–265.
4. MacKenzie-Graham A, Kurth F, Itoh Y, et al. Disability-specific atlases of gray matter loss in relapsing-remitting multiple sclerosis. JAMA Neurol 2016;73:944–953.
5. Wang M, Gao M, Miller KD, Zheng QH. Synthesis of [(1)(1)C]PBR06 and [(1)(8)F]PBR06 as agents for positron emission tomographic (PET) imaging of the translocator protein (TSPO). Steroids 2011;76:1331–1340.
6. Singhal T, Weiner HL, Bakshi R. TSPO-PET imaging to assess cerebral microglial activation in multiple sclerosis. Semin Neurol 2017;37:546–557.
7. Lartey FM, Ahn GO, Shen B, et al. PET imaging of stroke-induced neuroinflammation in mice using [18F]PBR06. Mol Imaging Biol 2014;16:109–117.
8. James ML, Belichenko NP, Nguyen TV, et al. PET imaging of translocator protein (18 kDa) in a mouse model of Alzheimer's disease using N-(2,5-dimethoxybenzyl)-2-18F-fluoro-N-(2-phenoxyphenyl)acetamide. J Nucl Med 2015;56:311–316.
9. Singhal T, O'Connor K, Dubey S, et al. 18F-PBR06 versus 11C-PBR28 PET for assessing white matter translocator protein binding in multiple sclerosis. Clin Nucl Med 2018;43:e289–e295.
10. Lublin FD, Reingold SC, Cohen JA, et al. Defining the clinical course of multiple sclerosis: the 2013 revisions. Neurology 2014;83:278–286.
11. Meier DS, Guttmann CRG, Tummala S, et al. Dual-sensitivity multiple sclerosis lesion and CSF segmentation for multichannel 3T brain MRI. J Neuroimaging 2018;28:36–47.
12. Kim G, Chu R, Yousuf F, et al. Sample size requirements for one-year treatment effects using deep gray matter volume from 3T MRI in progressive forms of multiple sclerosis. Int J Neurosci 2017;127:971–980.
13. Dupuy SL, Tauhid S, Hurwitz S, Chu R, Yousuf F, Bakshi R. The effect of dimethyl fumarate on cerebral gray matter atrophy in multiple sclerosis. Neurol Ther 2016;5:215–229.
14. Chu R, Tauhid S, Glanz BI, et al. Whole brain volume measured from 1.5T versus 3T MRI in healthy subjects and patients with multiple sclerosis. J Neuroimaging 2016;26:62–67.
15. Tzourio-Mazoyer N, Landeau B, Papathanassiou D, et al. Automated anatomical labeling of activations in SPM using a macroscopic anatomical parcellation of the MNI MRI single-subject brain. NeuroImage 2002;15:273–289.
16. Penny W, Friston K, Ashburner J, Kiebel S, Nichols T. Statistical Parametric Mapping. The Analysis of Functional Brain Images. London: Elsevier Ltd; 2007.
17. Politis M, Giannetti P, Su P, et al. Increased PK11195 PET binding in the cortex of patients with MS correlates with disability. Neurology 2012;79:523–530.
18. Herranz E, Gianni C, Louapre C, et al. Neuroinflammatory component of gray matter pathology in multiple sclerosis. Ann Neurol 2016;80:776–790.
19. Vercellino M, Masera S, Lorenzatti M, et al. Demyelination, inflammation, and neurodegeneration in multiple sclerosis deep gray matter. J Neuropathol Exp Neurol 2009;68:489–502.
20. Mahad DH, Trapp BD, Lassmann H. Pathological mechanisms in progressive multiple sclerosis. Lancet Neurol 2015;14:183–193.
21. Geurts JJ, Reuling IE, Vrenken H, et al. MR spectroscopic evidence for thalamic and hippocampal, but not cortical, damage in multiple sclerosis. Magn Reson Med 2006;55:478–483.
22. Azevedo CJ, Cen SY, Khadka S, et al. Thalamic atrophy in multiple sclerosis: a magnetic resonance imaging marker of neurodegeneration throughout disease. Ann Neurol 2018;83:223–234.
23. Neema M, Arora A, Healy BC, et al. Deep gray matter involvement on brain MRI scans is associated with clinical progression in multiple sclerosis. J Neuroimaging 2009;19:3–8.
24. Rissanen E, Tuisku J, Rokka J, et al. In vivo detection of diffuse inflammation in secondary progressive multiple sclerosis using PET imaging and the radioligand 11C-PK11195. J Nucl Med 2014;55:939–944.
25. Banati RB, Newcombe J, Gunn RN, et al. The peripheral benzodiazepine binding site in the brain in multiple sclerosis: quantitative in vivo imaging of microglia as a measure of disease activity. Brain 2000;123(pt 11):2321–2337.
26. Schweser F, Raffaini Duarte Martins AL, Hagemeier J, et al. Mapping of thalamic magnetic susceptibility in multiple sclerosis indicates decreasing iron with disease duration: a proposed mechanistic relationship between inflammation and oligodendrocyte vitality. Neuroimage 2018;167:438–452.
27. Geurts JJ, Bö L, Roosendaal SD, et al. Extensive hippocampal demyelination in multiple sclerosis. J Neuropathol Exp Neurol 2007;66:819–827.
28. Papadopoulos D, Dukes S, Patel R, Nicholas R, Vora A, Reynolds R. Substantial archaeocortical atrophy and neuronal loss in multiple sclerosis. Brain Pathol 2009;19:238–253.
29. Howell OW, Reeves CA, Nicholas R, et al. Meningeal inflammation is widespread and linked to cortical pathology in multiple sclerosis. Brain 2011;134:2755–2771.
30. Steenwijk MD, Geurts JJ, Daams M, et al. Cortical atrophy patterns in multiple sclerosis are non-random and clinically relevant. Brain 2016;139:115–126.
31. Colasanti A, Guo Q, Giannetti P, et al. Hippocampal neuroinflammation, functional connectivity, and depressive symptoms in multiple sclerosis. Biol Psychiatry 2016;80:62–72.
32. Rubio-Garrido P, Perez-de-Manzo F, Porrero C, Galazo MJ, Clasca F. Thalamic input to distal apical dendrites in neocortical layer 1 is massive and highly convergent. Cereb Cortex 2009;19:2380–2395.
33. Kern KC, Gold SM, Lee B, et al. Thalamic-hippocampal-prefrontal disruption in relapsing-remitting multiple sclerosis. Neuroimage Clin 2015;8:440–447.
34. Chitnis T, Weiner HL. CNS inflammation and neurodegeneration. J Clin Invest 2017;127:3577–3587.
35. Dutta R, Trapp BD. The pathology of multiple sclerosis. In: Cohen J, Rudick RA, editors. Multiple Sclerosis Therapeutics. 4th ed. Cambridge: Cambridge University Press; 2011:17.
36. Bar-Or A, Darlington PJ. The immunology of multiple sclerosis. In: Cohen J, Rudick RA, editors. Multiple Sclerosis Therapeutics. 4th ed. Cambridge: Cambridge University Press; 2011:20–34.
37. Trapp BD, Stys PK. Virtual hypoxia and chronic necrosis of demyelinated axons in multiple sclerosis. Lancet Neurol 2009;8:280–291.
38. Peterson JW, Bö L, Mörk S, Chang A, Trapp BD. Transected neurites, apoptotic neurons, and reduced inflammation in cortical multiple sclerosis lesions. Ann Neurol 2001;50:389–400.
39. Lagumersindez-Denis N, Wrzos C, Mack M, et al. Differential contribution of immune effector mechanisms to cortical demyelination in multiple sclerosis. Acta Neuropathologica 2017;134:15–34.